



HAL
open science

Cascading Effects of Extreme Geohazards on Tenerife (Canary Islands)

Marta López-saavedra, Joan Martí, Jose Luis Rubio, Karim Kelfoun

► **To cite this version:**

Marta López-saavedra, Joan Martí, Jose Luis Rubio, Karim Kelfoun. Cascading Effects of Extreme Geohazards on Tenerife (Canary Islands). *Journal of Geophysical Research: Solid Earth*, 2021, 126 (9), 10.1029/2021JB022294 . hal-03524228

HAL Id: hal-03524228

<https://uca.hal.science/hal-03524228>

Submitted on 13 Jan 2022

HAL is a multi-disciplinary open access archive for the deposit and dissemination of scientific research documents, whether they are published or not. The documents may come from teaching and research institutions in France or abroad, or from public or private research centers.

L'archive ouverte pluridisciplinaire **HAL**, est destinée au dépôt et à la diffusion de documents scientifiques de niveau recherche, publiés ou non, émanant des établissements d'enseignement et de recherche français ou étrangers, des laboratoires publics ou privés.

Cascading Effects of Extreme Geohazards on Tenerife (Canary Islands)



Key Points:

- Tenerife is a good example of where cascading extreme hazards have occurred several times in the past and could occur again in the future
- The modeling of a multi-hazard scenario enables us to predict the potential extent and impact of a caldera-forming eruption on Tenerife
- A long-term multi-hazard assessment of Tenerife shows the impact that a sequence of extreme events could have beyond the Canary Islands

Supporting Information:

Supporting Information may be found in the online version of this article.

Correspondence to:

M. López-Saavedra,
mlopez@geo3bcn.csic.es

Citation:

López-Saavedra, M., Martí, J., Rubio, J. L., & Kelfoun, K. (2021). Cascading effects of extreme geohazards on Tenerife (Canary Islands). *Journal of Geophysical Research: Solid Earth*, 126, e2021JB022294. <https://doi.org/10.1029/2021JB022294>

Received 6 MAY 2021

Accepted 6 SEP 2021

Marta López-Saavedra¹ , Joan Martí¹ , Jose Luis Rubio², and Karim Kelfoun³ 

¹Geosciences Barcelona, CSIC, Barcelona, Spain, ²Department of Geology, University Autonomus of Barcelona, UAB, Bellaterra, Spain, ³Laboratoire Magmas et Volcans, Université Clermont Auvergne, CNRS, IRD, OPGC, Aubin, France

Abstract Extreme geohazards (volcanic eruptions, earthquakes, landslides, and tsunamis) have the potential to inflict cascading effects whose associated risks are difficult to predict and prepare for. Thus, these events are generally not taken into account in hazard assessment. Anticipating the occurrence of such extreme events is thus key if our life-styles are to remain safe and sustainable. Volcanic islands are often the source of complex successions of disastrous events, as is evident from any examination, for instance, of the geological record of regions such as Hawaii, the Canary Islands, Reunion and Indonesia. The island of Tenerife in the Canary Archipelago is an excellent example of where cascading extreme hazards have occurred several times in the past and could occur again in the future. A cascading sequence involving a caldera-forming eruption, high-magnitude seismicity, mega-landslides and tsunamis occurred at least twice during the construction of this island. In order to understand the possible consequences of such processes if they were to reoccur, we simulated the extent and potential impact of a multiple, extreme geohazard episode similar to the last recorded one that took place on the island of Tenerife around 180 ka. The implications of such a disastrous succession of events are analyzed at local, regional and global scales, and the results obtained are discussed within the framework of disaster risk-reduction policies.

Plain Language Summary Extreme geohazards are geological events (e.g., volcanic eruptions, earthquakes, landslides, or tsunamis) that pose a serious risk for our globalized and technology-dependent society, and could potentially have a significant impact both locally and globally. Volcanic islands are large volcanoes that have grown out from the seafloor whose tops have emerged above sea level to form islands, on which a chain or succession of disasters (cascading events) could occur. Successions involving large explosive eruptions leading to the collapse of the central part of a volcano into its magma chamber, thereby forming a collapse caldera and provoking high-magnitude earthquakes, mega-landslides and tsunamis, occurred several times during the evolution of Tenerife, the largest volcanic island in the Canary Archipelago, and could occur again in the future. To understand the consequences if such an event occurred today, we modeled the most recent succession of extreme geological events that occurred on Tenerife about 180,000 years ago. The results obtained are analyzed at local, regional and global scales, and are relevant to the emergency plans that need to be developed to confront volcanic and associated risks in the Canary Islands and other similar regions.

1. Introduction

Extreme geohazards (super-eruptions, earthquakes, mega-landslides, and tsunamis) are low-probability high-impact events with the potential to inflict cascading effects, whose associated risks are difficult to predict and prepare for (Lee et al., 2012; Nott, 2006; Plag et al., 2013; Ranke, 2016; Sharma et al., 2012). These types of events are characterized by their short unfolding time but much longer impact time, with the potential to generate global disasters. Thus, they are generally not taken into account in hazard assessment and, consequently, they are usually underestimated in disaster risk-reduction studies and policies (Plag et al., 2013).

However, the eruption of Eyjafjallajökull volcano in Iceland in 2010 showed that today even a small recurrent event could have an impact worldwide due to the greater complexity of our society (Lee et al., 2012; Plag et al., 2013). Modern civilisation's lack of experience in extreme events, together with the rise in population density, has increased our exposure to geohazards since, for instance, many megacities and industries

© 2021. The Authors.

This is an open access article under the terms of the [Creative Commons Attribution-NonCommercial-NoDerivs License](https://creativecommons.org/licenses/by-nc-nd/4.0/), which permits use and distribution in any medium, provided the original work is properly cited, the use is non-commercial and no modifications or adaptations are made.

are located in hazardous areas. Recent efforts, such as the analysis made by Patrick et al. (2020) on the 2018 Kilauea eruption, have highlighted the importance of the study of cascading hazards for future forecasting, given the magnitude and complexity of their consequences.

Volcanic islands are good examples of fragile economic systems and highly vulnerable communities whose main monetary income is from tourism and local economic activities such as fishing and agriculture. Created by the growth of volcanoes in the sea and modified by natural and anthropogenic processes, volcanic islands are subject to the impact of multiple natural hazards, including extreme geohazards, as well as forest fires, storms and floods. Given their intrinsic multi-hazard nature, volcanic eruptions are the most common extreme geohazards liable to trigger concatenated effects in this type of environment. Tenerife is an excellent example of a site exposed to cascading extreme geohazards that have occurred several times in the past and could occur again in the future, since the geophysical conditions that determine the occurrence of such catastrophic events are still present. A cascading sequence of a caldera-forming eruption, high-magnitude seismicity, a mega-landslide and a tsunami occurred at least twice during the construction of the central and eastern sectors of the caldera of Las Cañadas, and gave rise to the Orotava and Icod valleys. Despite being the most populated island in the archipelago and receiving millions of tourists every year, no detailed multi-hazard assessment has ever been conducted for Tenerife.

In order to fill the gap in the information necessary for correct emergency planning for the island and the rest of the region, we conduct this initial long-term multi-hazard assessment. The aim of this study is to quantify the extent and potential impact of an episode of multiple extreme geohazards similar to the one that occurred on Tenerife around 180 ka if it occurred today. We first review the stratigraphic evidence to determine the temporal succession of events and the relationship of cause and effect. Then, we analyze each of the processes that occurred during the succession separately, but considering the nature and consequences of the possible relationship between the described events. To do this, we describe the main characteristics, magnitude and area of occurrence and impact of each hazard, but we adjust some of these properties depending on the results obtained from the previous event along the cascading simulation. This linkage has been done specially for the seismicity-landslide and landslide-tsunami sequence pairs. We also take into account the current topography of the island and its demographic distribution to assess the potential impact of the multi-hazard scenario. Then, we analyze the overall result of all the simulated scenarios to quantify the potential extent and impact of the occurrence of these multi-hazards today. Finally, we examine the implications of this multi-hazard scenario at local, regional and global scales, and discuss the results obtained within a framework of disaster risk reduction policies.

2. Geological Setting

Tenerife is the largest of the Canary Islands, an intra-plate volcanic archipelago connected to a long-lasting mantle plume whose structure and geodynamic evolution still evoke considerable debate (e.g., Anguita & Hernan, 1975, 2000; Araña & Ortiz, 1991; Carracedo et al., 1998; Fullea et al., 2015; Hernández-Pacheco & Ibarrola, 1973; Hoernle & Schmincke, 1993; Schmincke, 1982). The geological evolution of Tenerife involved the construction of two principal volcanic complexes (Figure 1): a basaltic shield complex (>12 Ma to present, Abdel-Monem et al., 1972; Ancochea et al., 1990; Thirlwall et al., 2000) and a central complex (<4 Ma to present, Ancochea et al., 1990; Araña, 1971; Fuster et al., 1968; Martí, Mitjavila, & Araña, 1994). The basaltic shield complex is mostly submerged and forms about 90% of the volume of the island; its sub-aerial construction continues at present through two rift zones (Santiago Rift Zone and Dorsal Rift Zone) and in a broad monogenetic volcanic field to the south of the island. The central complex corresponds to Las Cañadas edifice (<4–0.18 Ma), a composite volcano characterized by abundant explosive eruptions of highly evolved phonolitic magmas, and the active Teide-Pico Viejo twin stratovolcanoes (0.18 ka-present). The formation of the caldera of Las Cañadas, of which the Teide-Pico Viejo stratovolcanoes are part (Figure 1c), truncated the edifice of Las Cañadas, which was transformed by several vertical collapses occasionally associated with lateral collapses on the volcano's flanks (Martí & Gudmundsson, 2000; Martí, Mitjavila, & Araña, 1994; Martí et al., 1997).

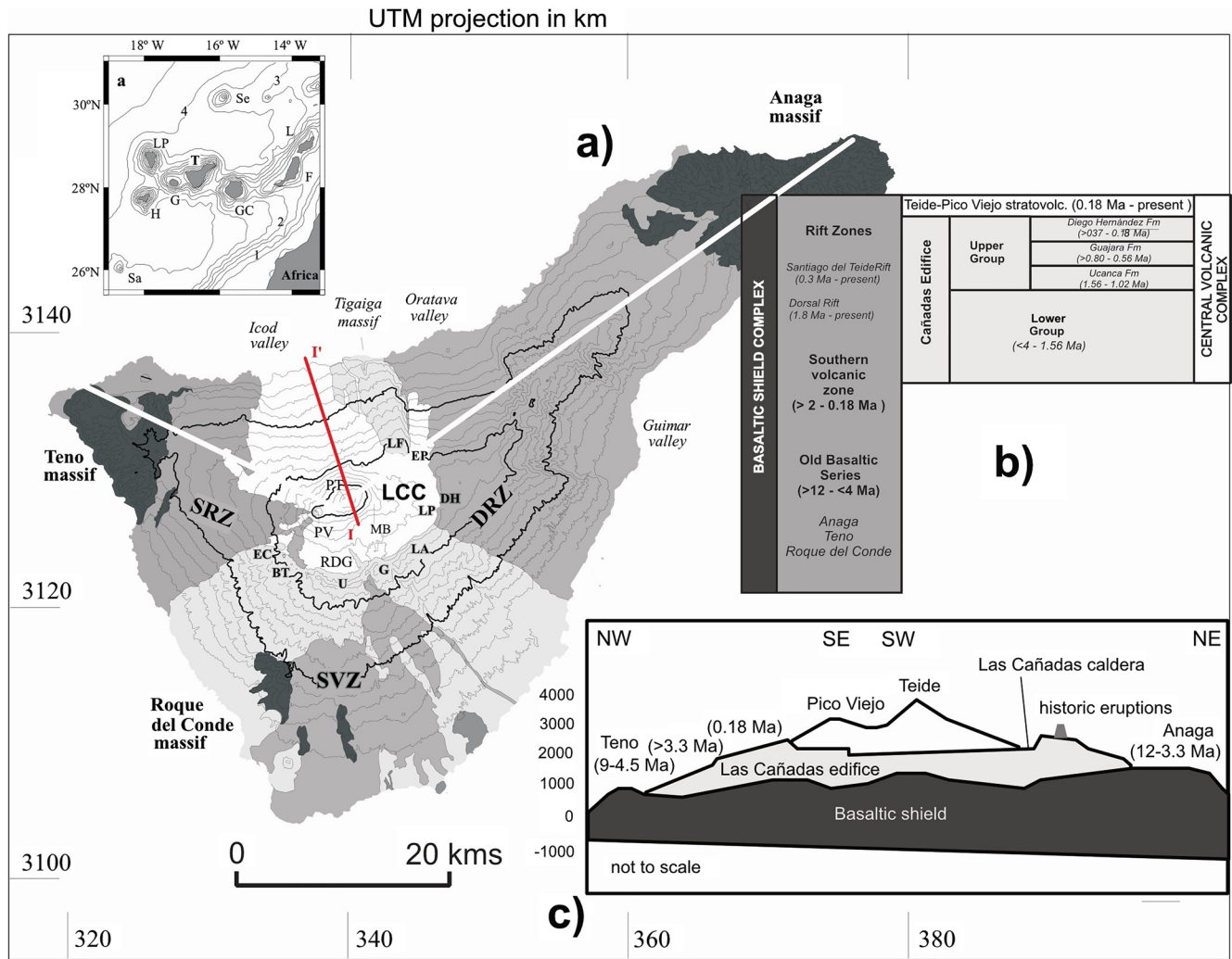


Figure 1. (a) Simplified geological map of Tenerife (modified from Ablay & Martí, 2000), (b) stratigraphy of Tenerife and (c) schematic cross-section of the island. Las Cañadas caldera wall localities: EC-El Cedro; BT-Boca Tauce; U-Ucanca; RDG-Roques de García; G-Guajara; LA-Las Angosturas; LP-Las Pilas; DH-Diego Hernández; EP-El Portillo; LF-La Fortaleza. Main vent systems of the Teide-Pico Viejo formation: PT-Teide volcano; PV-Pico Viejo volcano; MB-Montaña Blanca. Post-shield mafic volcanic zones: SRZ-Santiago rift zone; DRZ-Dorsal rift zone; SVZ-Southern volcanic zone (locally known as Bandas del Sur). Names and locations of landslide valleys are also shown. Contour interval is 200 m. Isotopic ages are from Ancochea et al. (1990) and Martí, Mitjavila, and Araña (1994). Inset map shows the location and distribution of the Canary Islands. Main islands: LP-La Palma; EH-El Hierro; G-La Gomera; T-Tenerife; GC-Gran Canaria; F-Fuerteventura; L-Lanzarote. The white lines correspond to the cross-section of part (c) of this figure, and the red line I-I' corresponds to the cross-sections in Figures 2 and 3.

2.1. Stratigraphic Relationships Between Extreme Geohazards on Tenerife

A change in the eruptive dynamics of Tenerife between 2 Ma and 1.5 Ma initiated a period consisting of three long-term cycles of phonolitic explosive activity, with volumetrically larger and more extensive eruptions, that constructed Las Cañadas edifice Upper Group and ranges from 1.57 to 0.17–0.18 Ma (Ancochea et al., 1990, 1999; Boulesteix et al., 2012; Brown et al., 2003; Bryan et al., 1998; Edgar et al., 2007; Huertas et al., 2002; Martí, Mitjavila, & Araña, 1994; Mitjavila & Villa, 1993). Each of these phonolitic volcanic cycles terminated with a caldera collapse episode (Martí, 2019; Martí & Gudmundsson, 2000; Martí, Mitjavila, & Araña, 1994).

During the construction of Las Cañadas, several large sector collapses affected parts of the island, at least two of which coincided in time with the occurrence of caldera-forming episodes. This is the case of La Oratava and Icod valleys, on the northern flank of Tenerife, which are coeval with the formation of the central (Guajara, 0.56 Ma) and eastern (Diego Hernández, 0.17 Ma) sectors of the caldera, respectively (Carracedo

et al., 2011; Hunt et al., 2011, 2013a, 2013b, 2018; Ibarrola et al., 1993; Martí, 2019; Martí et al., 1997; Martí & Gudmundsson, 2000).

The formation of the Icod valley coincided with the eruption of El Abrigo (Boulestex et al., 2012; Hunt et al., 2011; Martí, Mitjavila, & Araña, 1994; Martí et al., 1997; Paris et al., 2017), the caldera-forming eruption that culminated the final phonolitic cycle of the Upper Group (0.179 Ma, Martí, Mitjavila, & Araña, 1994). According to Martí (2019), the inland stratigraphy of the related deposits reveals the temporal sequence of these catastrophic events and contrasts with that proposed by other authors (e.g., Hunt et al., 2018; Paris et al., 2017). The lack of El Abrigo deposits in the Icod valley contrasts with their presence throughout the rest of the island in a continuous 2–20 m-thick layer (Pittari, 2004; Pittari et al., 2008), which indicates that this eruption preceded the subaerial landslide. The landslide may have started on the submarine flanks during the unrest period preceding the eruption (Hunt et al., 2011, 2013a, 2013b, 2018), probably as a response to strong continuous seismicity and ground deformation caused by the inflation of the associated magma chamber (Andújar et al., 2008; Martí, 2019). This initial submarine landslide, involving volumes of 240–264 km³ (Hunt et al., 2011, 2013a, 2013b, 2018), would have continued on land during the caldera collapse episode and led to the removal of approximately 60 km³ of the northern sector of the volcanic edifice (Iribarren, 2014). The result would have been a multistage retrogressive failure with stages separated by periods of several days (Hunt et al., 2011; Paris et al., 2017).

The subaerial landslide would have caused a tsunami whose deposits are preserved in thicknesses of 0.4–3 m on the north-west flanks of Tenerife at altitudes up to 132 m a.s.l. (Paris et al., 2017). A characteristic of these tsunami deposits found on the northern coast of Tenerife is that they contain pumice clasts from El Abrigo (Paris et al., 2017). This indicates that the tsunami and, consequently, the landslide that originated it, occurred once the eruption had ended or whilst it was still underway and the pumices were already deposited and floating on the surface of the sea.

An avalanche breccia, known as “Mortalón”, with an inclination of 9.42° in Icod (Iribarren, 2014) and interpreted by Bravo (1962) and Coello (1973) as an old breccia deposit generated by previous mass wasting processes affecting the basaltic shield and the beginning of the construction of the Las Cañadas edifice, is thought in fact to represent the décollement surface for both La Orotava and Icod landslides.

Hürlimann et al. (2000) proposed adjacent and shallow seismic shocks caused by the seismogenic slip on the ring fault originated by the caldera collapse as the main driving forces triggering the large-scale subaerial slope failure; such shocks are capable of applying faster and more dynamic stress to slopes than other mechanisms such as dike intrusion (e.g., McGuire et al., 1990; Voight & Elsworth, 1997) and the inflation and deflation of the magma chamber (e.g., Lo Giudice & Rasa, 1992). According to stability analyses, an unstable state is reached for a seismic shock with a horizontal acceleration over 0.3 g. Assuming a magnitude of 5.0 for a seismic shock related to the caldera collapse at a distance of 5 km, a maximum horizontal acceleration coefficient (PHAC) of 0.29 would be generated (Hürlimann et al., 2000). Comparing these results with other observational data from some recent calderas (e.g., Abe, 1992; Alvizuri et al., 2020; Filson et al., 1973; Riel et al., 2015), a *M_w* magnitude of 5–7.2 is required for seismic shocks to have triggered the Icod landslide (Hürlimann et al., 2000).

3. Methodology

To conduct the multi-hazard assessment corresponding to a hypothetical repetition today of the same succession of events that took place on Tenerife about 0.18 Ma, it is necessary to simulate scenarios that reproduce all the volcanic and associated hazards that occurred during the caldera-forming eruption of El Abrigo. This will help predict which areas could be affected by each of these processes. The objective was to combine freely available models and commercial software with Geographic Information Systems (GIS) to model and analyze the various potential hazards and so identify their current potential extent and impact. According to the succession of events deduced from the geological record and, in particular, from the inland stratigraphy (Martí, 2019), the following hazards need to be simulated: pyroclastic density currents (PDC), seismicity, landslide and tsunami. Ash fallout has not been identified on Tenerife in association with El Abrigo eruption (Pittari, 2004), although it is likely that a considerable co-ignimbrite ash cloud developed

during the emplacement of the ignimbrite from El Abrigo. Nevertheless, no data exist to indicate its size or extent and so this hazard has not been modeled.

PDC simulations were conducted using VORIS 2.0.1. (Felpeto et al., 2007, available at <http://www.gvb-csic.es/GVB/VORIS/VORIS.htm>), a GIS-based tool for volcanic hazard assessment that includes several simulation models. The PDC simulation model used is based on the Energy Cone model (Malin & Sheridan, 1982; Sheridan & Malin, 1983) and the modification by Toyos et al. (2007), and is able to calculate the runout, velocity and dynamic pressure of pyroclastic flows. Simulations of the Peak Ground Acceleration (PGA) caused by seismicity induced by caldera collapse were performed automatically using a plugin developed by Núñez (2017) implemented in the Geographic Information System QGIS, 2.14 version. Landslide simulations were conducted using the commercial software SLIDE, developed by Rocscience Inc. (Rocscience Inc., 2020, <https://www.rocscience.com/software/slope-stability>) for slope stability analyses. Finally, the tsunami was simulated using VolcFlow (Kelfoun & Druitt, 2005)

As input parameters for all these simulations the current topography of Tenerife consisting of a 50-m resolution Digital Elevation Model provided by the National Geographic Institute (IGN, www.ign.es) was used, in combination with the digital bathymetry around the Canary Islands at the same resolution generated by the Spanish Institute of Oceanography (IEO, www.ieo.es). Given that one of the objectives was to reproduce the extent of the ignimbrite deposited after El Abrigo that nearly buried the whole island of Tenerife (Pittari, 2004; Pittari et al., 2008), up to seven different collapse equivalent angles (α_c) (4° — for base surge explosions —, 7° , 11° , 15° , 19° , 23° and 27° — for column collapse phases —) (Sheridan & Malin, 1983), and a collapse equivalent height (H_c) of 2,000 and 3,000 m, respectively, were considered in a trial and error application of the PDC simulation model. All the simulations were conducted assuming a single eruptive area located in the current crater of Mt Teide.

Following Núñez (2017), the geological units represented on the geological map GEODE 1:25000 from Tenerife (2913 zone) (Bellido-Mulas et al., 2014) were classified in six groups to elaborate a seismic amplification map of Tenerife (Supporting Information S1), according to the methodology developed by Borchardt (1994) (more information in Text S1). We assumed that the seismic shocks triggered by a caldera collapse have their hypocenters along the ring faults that control the vertical movement of the block that is collapsing. It is also well known that the position and extent of a collapse caldera are limited by the position and extent of the associated magma chamber (Folch & Martí, 2009; Martí, Ablay, Redshaw, & Sparks, 1994; Martí et al., 2008). For this reason, the position of the hypothetical magma chamber in the case simulated here will determine the position of the ring faults and hence the position of the possible hypocenters and/or epicenters. The magma chamber at the time of El Abrigo eruption is assumed to have had a total volume of at least 20 km^3 (this is the minimum erupted volume; Martí, Mitjavila, & Araña, 1994; Pittari, 2004), to have been about 5 km in diameter given the size of the resulting depression (Coppo et al., 2008; Martí, Mitjavila, & Araña, 1994), and to have been located about 4 km below surface at the time of the eruption (Andújar et al., 2008). Two positions for the magma chamber were assumed in our simulations (Figure 2) and three hypocenters were considered for each epicenter given current topography and the depth of the magma chamber (Figure 2), which thus give rise to a total of six possible locations for the seismic focuses. For each focus, three moment magnitudes (M_w) were used ($M_w = 5, 6, \text{ and } 7$), values that are within the observed common range for these type of eruptive seismic shocks (Hürlimann et al., 2000). Finally, the simulation of the seismic scenarios was performed by applying three attenuation laws following our geotechnical classification of materials. All of the input parameters are shown in Table 1.

By taking into account the estimated earthquake magnitudes that could have triggered the Icod landslide (Hürlimann et al., 2000), slope stability simulations were carried out considering the current topography, stratigraphy and geotechnical properties. We used SLIDE (Rocscience Inc., 2020), a 2D limit equilibrium slope stability program, to evaluate the Factor of Safety (FS) or probability of failure, of circular or non-circular failure surfaces on soil or rock slopes. This program uses different limit equilibrium methods designed to investigate the equilibrium of a soil or a rock mass tending to slide down under the influence of gravity. These methods compare forces, moments, or stresses resisting movement of the mass for a given geotechnical configuration, with disturbing forces, such as those produced by an earthquake. As a result, the program calculates the FS of the slope and reveals the most probable slip surfaces. Two simplified contrasting models (Model 1, Figure 3a and Model 2, Figure 3b) based on the cross-sections drawn by Carracedo et al. (2007),

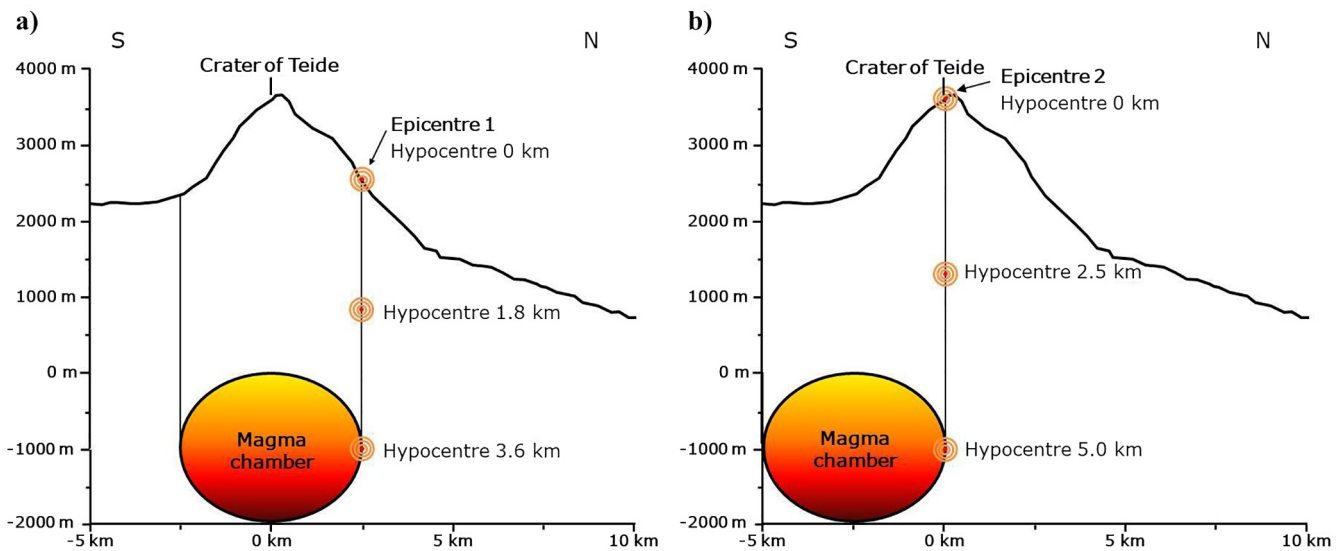


Figure 2. Simplified cross section of Mt Teide (S–N) showing the two presumed positions of the magma chamber (>20 km³, 5-km wide, 4-km deep) and their respective epicenters and hypocenters proposed for the earthquake simulations: (a) a magma chamber located just below the crater of Mt Teide and (b) a magma chamber displaced to the south whose the northern limit would be below the crater. The line corresponding to this cross-section is part of the red line I–I' shown in Figure 1.

Marrero (2010) and Martí (2019) were designed to evaluate the stability of the northern slope of Tenerife according to the geotechnical classification of volcanic materials in Del Potro and Hürlimann (2008).

In order to simplify the model, infinite strength was assumed for fresh lavas from the basaltic shield as there was no landslide after the formation of the Las Cañadas edifice. Thus, these lavas represent a slip surface “exclusion zone” through which slip surfaces cannot penetrate. The Drained-Undrained option was used for both the “Mortalón” and the Las Cañadas edifice intracaldera materials, as it defines a soil strength envelope that considers both drained and undrained Mohr-Coulomb strength parameters, that is, effective and total parameters, for materials whose response to a seismic shock is unknown. For the rest of units considered as “rocks” (including the altered lavas from Mt Teide, which were characterized as an intermediate material between rock and soil based on their geotechnical characteristics), the Generalized Hoek-Brown strength criterion was applied, which works well for most rock masses of reasonable or low quality in which the rock mass strength is controlled by tightly interlocking angular rock pieces (Rocscience Inc., 2020). All inputs of geotechnical parameters are shown in Table 2.

The SLIDE software package enables different methods of vertical slice limit equilibrium analysis to be applied. These methods discretize the soil or rock mass above the assumed failure surface into vertical slices or columns with equal widths. In each column, force and moment equilibrium are held, at the same time that internal forces due to the interaction between the slices are considered. For this study, only three methods were used since Rocscience Inc. recommends that the others are not used as they do not fit the reality of our case of study: Bishop’s simplified method, which satisfies only moment equilibrium and considers interslice

Table 1
Input Parameters for Peak Ground Acceleration Simulations

Epicenter 1		Epicenter 2		M _w	Attenuation laws ^a
Location	Hypocenters	Location	Hypocenters		
lat = 28.294332°	0 km	lat = 28.272319°	0 km	5	Pétursson and Vogfjörd (2009)
lon = -16.650575°	1.8 km	lon = -16.642437°	2.5 km	6	Ágústsson et al. (2008)
	3.6 km		5 km	7	Beauducel et al. (2004)

^aNúñez (2017) states that the most accurate attenuation laws for Canary Islands are those given by Ágústsson et al. (2008), Beauducel et al. (2004) and Pétursson and Vogfjörd (2009) since they were built using accelerations observed in Iceland and on the island of Guadalupe, which are also volcanic environments.

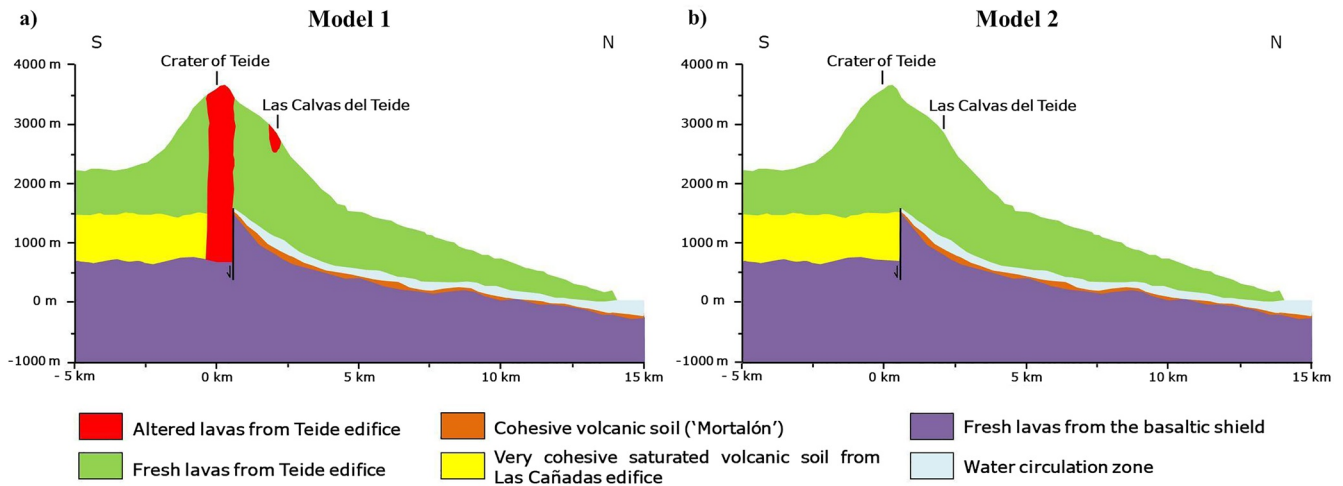


Figure 3. Simplified geotechnical S–N cross-sections in the north of Tenerife proposed for the slope stability analysis. (a) Model 1 considers alteration zones shown in red; (b) Model 2 does not consider alteration zones. See red line I–I' in Figure 1 for the line of the S–N cross-section. Based on Carracedo et al. (2007), Marrero (2010) and Martí (2019).

Table 2
Input Parameters for SLIDE Software

Parameter	Geotechnical units					
	Fresh lavas from the basaltic shield	Las Cañadas collapsed material	Mortalón	Water circulation zone	Fresh lavas from Mt Teide	Altered lavas from Mt Teide
Type	Rock	Soil	Soil	Rock	Rock	Rock/Soil
Strength criterion	Infinite strength	Drained-Undrained	Drained-Undrained	Gen. Hoek-Brown	Gen. Hoek-Brown	Gen. Hoek-Brown
Unit weight (kN/m ³)	24.6 ± 2.3 ^a	14.9 ^a	17.1 ± 2 ^a	22.6 ^b	24.6 ± 2.3 ^a	22.2 ± 3 ^a
Saturated unit weight (kN/m ³)	-	16.9 ^c	21 ^c	24.6 ^c	24.6 ^c	23.6 ^c
Effective angle of internal friction (φ) (°)	-	35 ^d	20 ^d	-	-	-
Undrained cohesion (Cu) (kg/cm ²)	-	0.1 ^c	0.7 ^e	-	-	-
Effective cohesion (c') (kg/cm ²)	-	0.01 ^f	0.13 ^g	-	-	-
Uniaxial Compressive Strength (UCS) (MPa)	-	-	-	55 ^h	65 ^j	30 ^d
Geological Strength Index (GSI)	-	-	-	25 ⁱ	35 ⁱ	20 ⁱ
m _i	-	-	-	15 ⁱ	15 ⁱ	14 ⁱ
m _b	-	-	-	1.03 ^j	1.472 ⁱ	0.804 ⁱ
s	-	-	-	0.00024 ⁱ	0.00073 ⁱ	0.00013 ⁱ
a	-	-	-	0.313 ⁱ	0.5159 ^j	0.5437 ⁱ

Note. Error margins were ignored during simulations to simplify calculations. m_i is a material constant for intact rocks. m_b, s and a are rock mass material constants.

^aDel Potro and Hürliemann (2008). ^bAssumed using geological-geotechnical criteria. ^cAssumed using geological-geotechnical criteria based on the geological description in Del Potro and Hürliemann (2008). ^dConsidering conservative values from Hernández-Gutiérrez and Santamarta (2015) and assumed using geological-geotechnical criteria. ^eWeighted average from values provided by Uriel and Serrano (1975). ^fc'/Cu ratio = 0.1 (Rocscience Inc., 2020). ^gc'/Cu ratio = 0.186 (Rocscience Inc., 2020). ^hConservative values from those recommended by González de Vallejo et al. (2002) for intact rock from this type of material. ⁱRecalculated with RocData software (Rocscience Inc., 2020) under geological-geotechnical criteria. ^jArithmetic mean of the mean values of the simple compression tests corresponding to the basaltic type lithotypes from Hernández-Gutiérrez and Santamarta (2015), from a conservative perspective in terms of risk.

Table 3
k_h Values for the Selected Accelerations of Gravity According to the Pseudo-Static Analysis Criteria

Acceleration of gravity values (g)	<i>k_h</i>		
	Noda and Uwave (1976)	Marcuson (1981)	Saragoni (1993)
0.1	0.1	0.03	0.03
0.20	0.20	0.07	0.06
<u>0.67</u>	0.29	0.22	0.19
<u>3.35</u>	0.49	1.11	0.33
0.12	0.12	0.04	0.04
<u>0.49</u>	0.49	0.16	0.15
0.19	0.19	0.06	0.06
0.61	0.28	0.20	0.18
3.04	0.48	1.00	0.32
0.48	0.26	0.16	0.14
Extra value of <i>k_h</i>	0.13		

Note. PGA values in bold text were obtained from PGA simulations using Epicenter 1 (Figure 2a); underlined values in bold were obtained using Epicenter 2 (Figure 2b); the remaining values coincided with both epicenters.

shear forces as zero (Bishop, 1955); Janbu's Generalised method, which satisfies only force equilibrium but also considers interslice shear forces as zero (Janbu, 1973); and Morgenstern-Price method, which satisfies both moment and force equilibrium and considers variable interslice shear forces (Morgenstern & Price, 1965).

A static analysis was performed for both contrasting geotechnical models by applying the previous analytic methods to obtain the FS prior to an earthquake. Then, a pseudo-static analysis was performed for both models using the same methodology to analyze slope stability under seismic conditions. Since we were unable to simulate the whole caldera collapse process to determine how the seismicity produced by friction along the ring fault affects the Icod valley at each moment, we simulated the two extreme stages: at the beginning of the collapse, when the edifice is practically intact but some friction is occurring and so some seismic shocks are generated, and at the end, when the collapse is almost over and so the seismicity generated by the friction is about to end. Nevertheless, we are aware that the landslide could have occurred at any time during the collapse process and, although we do not know exactly when, we know from the stratigraphy that it occurred after the ignimbrite was emplaced. Hence, a third pseudo-static analysis was performed for Model 1 excluding the central part of the Mt Teide volcanic edifice. This simulated a collapse of that sector into the magma chamber during the formation of the caldera to test the slope stability of the Icod valley at the end of the collapse process. To do so, we used Model 1 as an input file for SLIDE software, but renamed it as "Model 1 Bis", and assumed the existence of

a magma chamber located just below the crater of Mt Teide corresponding to the configuration shown in Figure 2a. To achieve this, we moved one of the limits of the calculation zone considered by SLIDE 2.5 km to the north of the crater and restricted the calculation of the FS to the portion corresponding only to the Icod valley since it would not have any mass behind its head zone.

A total of 10 different maximum values of acceleration of gravity (g) were taken from the results obtained from the PGA simulations, and three formulas—those of Marcuson (1981) (1), Noda and Uwave (1976) (2) and Saragoni (1993) (3)—were applied to each PGA value to obtain 22 different horizontal seismic coefficient (*k_h*) values used in the SLIDE pseudo-static analysis.

$$k_h = \frac{0.33 * a_{max}}{g} \quad (1)$$

$$k_h = \frac{a_{max}}{g} \quad \text{If } a_{max} \leq 2 \text{ m/s}^2 \quad (2)$$

$$k_h = 0.33 * \left(\frac{a_{max}}{g} \right)^{0.33} \quad \text{If } a_{max} > 2 \text{ m/s}^2$$

$$k_h = 0.3 * \frac{a_{max}}{g} \quad \text{If } a_{max} \leq 6.6 \text{ m/s}^2 \quad (3)$$

$$k_h = 0.22 * \left(\frac{a_{max}}{g} \right)^{0.33} \quad \text{If } a_{max} > 6.6 \text{ m/s}^2$$

where *a_{max}* is the PGA as a fraction of the acceleration of gravity on Earth (g), and *g* = 1 in these formulas (Gutiérrez, 2017).

These 10 PGA values (Table 3) were selected after filtering the results from previous seismicity simulations (Tables S2 and S3); the variable "depth" was eliminated as PGA values did not vary with depth, as were all results for *M_w* = 7 since this magnitude is outside the range of applicability of the three attenuation laws, but it was tested as an upper limit. Repeated values were selected only once. The input seismic values for simulations are shown in Table 3. An extra value of *k_h* = 0.13 for Model 1 was included after a trial and

error analysis to search for the limit at which all three methods of analysis show slope instability. This was not necessary for either Model 2 or Model 1 Bis since the limit was found at $k_h = 0.15$ and $k_h = 0.29$, respectively, which were two of the previously selected values from PGA results. According to Eurocode 7 (AENOR, 2016) and the Basic Document on Structural Safety (DB-SE) of the Technical Building Code (CTE) (Ministerio de Fomento, 2006), a minimum FS of 1.5 is required for slope stability in static and permanent conditions, and 1.1 for seismic and permanent conditions. Below these values, the slope is considered unstable. However, a lower FS limit is known to be sometimes more suitable for big landslides/slopes or for slope stability analysis different than those made for building security. Thus, we determined unstable conditions when $FS < 1$, and short-term stable conditions when FS values were 1–1.5 after considering the geotechnical configuration of the sector of the island selected and the possible margin of error in our parameter selection.

According to the geological record, the powerful tsunami was the final event of the chain of cascading multi-hazards in this case study. A simulation of the tsunami was generated with the two-fluids version of VolcFlow (Kelfoun et al., 2010), which can simulate both an avalanche and an associated tsunami. VolcFlow is a finite difference Eulerian code based on a depth-averaged approach. It runs inside MATLAB and solves depth-averaged equations of mass and momentum using a topography-linked coordinate system in time and space. First, the area covered by the landslide was drawn using Surfer software, keeping approximately the limits of the sliding mass obtained with SLIDE, and then entered as a numerical code in a TIF file, along with the bathymetry file in a Surfer Grid format. A maximum thickness of 500 m for the sliding block was considered, since it is approximately the thickness of the sliding mass obtained with SLIDE during the simulation of the landslide in this study. This thickness coincides with the average thickness of the current fill of the Icod valley from the surface to the “Mortalón” layer (Figure 3), which is taken to be the decollement surface of the last mega-landslide (Bravo, 1962). Following Kelfoun et al. (2010), the rheology of the sliding material was defined by a density of the avalanche block of $2,500 \text{ kg/m}^3$ (Del Potro & Hürliemann, 2008). This approximately coincides with the one used for the geotechnical unit of the fresh lavas from Teide, which occupies most of the sliding mass, as it was seen during the landslide simulation. Two different values were also used for the constant retarding stress that is equivalent to the cohesion of rocks or to a yield strength (50,000 Pa and 100,000 Pa, reasonable values determined by Kelfoun & Druitt, 2005, and Kelfoun et al., 2010). This rheology was obtained by comparing the results of the model with natural deposits (Kelfoun & Druitt, 2005; Kelfoun et al., 2010). A dynamic viscosity of water of $0.001137 \text{ Pa} \cdot \text{s}$ and a density of water of $1,025 \text{ kg/m}^3$ were also assumed.

4. Results

In all, 277 different eruptive scenarios were obtained from the simulations performed for the four extreme hazards selected for this study, and they are all included in Supporting Information S1.

4.1. PDC Scenarios

In all, 14 scenarios were obtained by combining up to seven different values for a_c and two different values for H_c . The PDC map scenarios are shown in Figures S2–S15, and an example is shown as well in Figure 4; numerical results and implications are summarized in Table S1.

Results show that as the a_c decreases, the surface area covered by PDC deposits increases. PDCs scenarios obtained here go from the whole affectation of the island of Tenerife, produced by an a_c of 4° , regardless the H_c , to a minimum affected area of almost 200 km^2 and just over 300 km^2 concentrated around the vent, corresponding to the area of Las Cañadas caldera and surroundings, produced by an a_c of 27° and an H_c of 2,000 m. Between these two extremes, there is a wide range of results in terms of surface area covered and municipalities affected by ignimbrite that deserves to be taken into account (see Table S1). Changes in two or three degrees of a_c , or in 1,000 meters of H_c , result in a variation of some hundreds of square kilometers affected.

It is observed that the Las Cañadas wall, a natural barrier for some volcanic hazards, such as lava flows, would stop the PDCs produced by a column collapse with an a_c equal or higher than 27° and an H_c of 2,000 m or less. In case an H_c of 3,000 m occurred, an a_c above 27° should occur so that the PDC would not

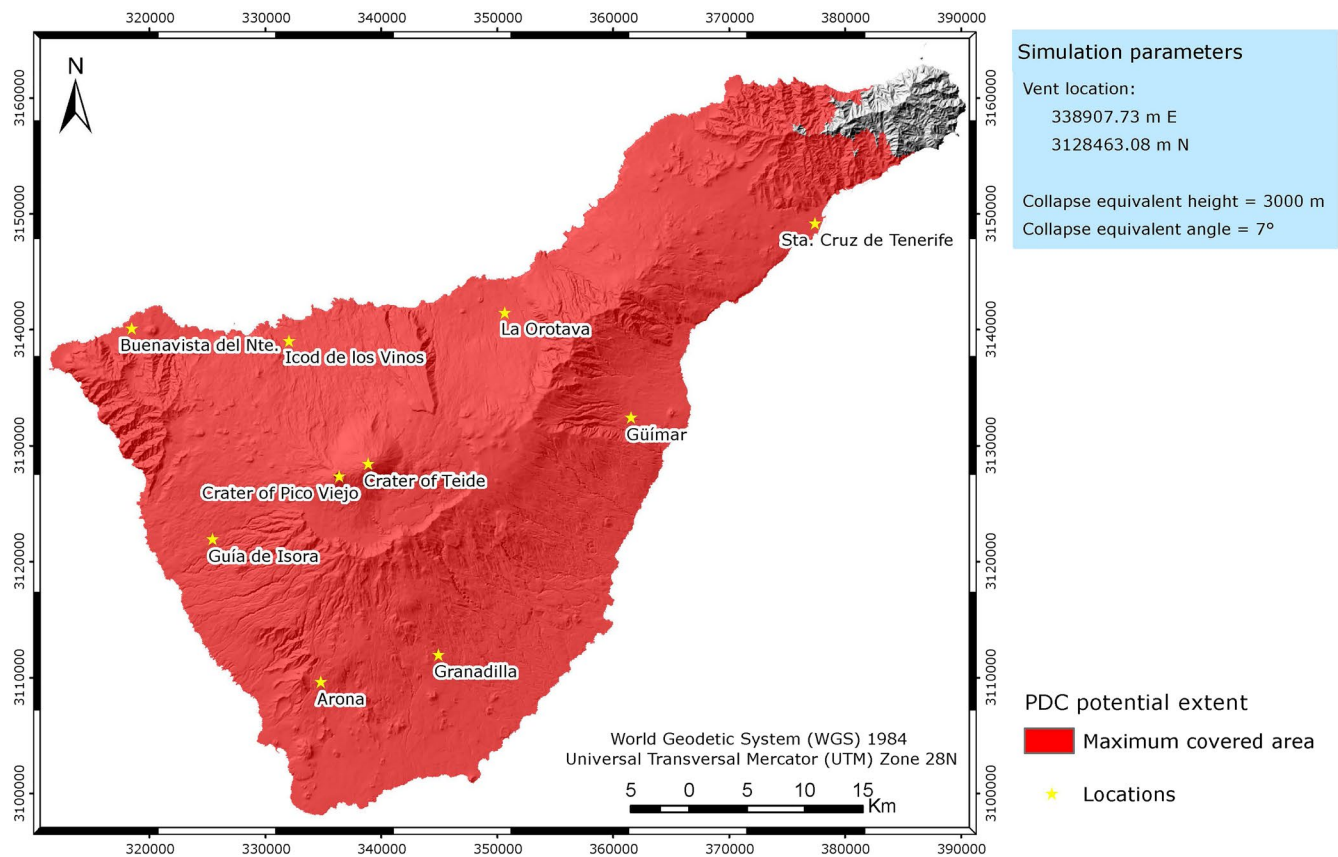


Figure 4. Pyroclastic Density Current map scenario considering $H_c = 3,000$ m and $a_c = 7^\circ$, for a simulated caldera-forming eruption on Mt Teide, Tenerife (Canary Islands).

exceed the limits of the central caldera. As there is no caldera wall towards the north, the most affected area after the Las Cañadas caldera is the Icod Valley.

Beyond this central topography, other topographic features, such as valleys, other cones, lava walls, basaltic shield remnants, could channel or act as barriers for pyroclastic flows, but this is observed in few more distal areas.

4.2. PGA Scenarios

In all, 54 scenarios were obtained combining three moment magnitudes (M_w), two different epicenters, each with three different hypocenters, and three attenuation laws. The maps of the expected PGA values are shown in Figures S16–S69, along with an example in the main text (Figure 5). Tables S2 and S3 summarize all the results.

Both epicenters give similar gravity acceleration values, even coinciding in some cases. Likewise, the modification of the hypocenter does not imply any change in these values. Only a slight increase in the expected PGA in cm/s^2 is observed as the hypocenter depth increases when applying the Beauducel et al. (2004) attenuation law, but these minor differences are eliminated when transforming the values into acceleration of gravity (g) units. The main differences in the expected PGA results are due to the M_w of the earthquake, but also to the chosen attenuation law.

Considering that a lower M_w would give a lower PGA, the lowest expected PGA values were obtained by applying the Pétursson and Vogfjörð (2009) attenuation law. In this case, PGA values go from 0.10 g (in case of both epicenters) to 0.29 g (in case of epicenter 1). At the other extreme, the highest expected PGA values, keeping all other parameters unchanged, were obtained after applying the Ágústsson et al. (2008)

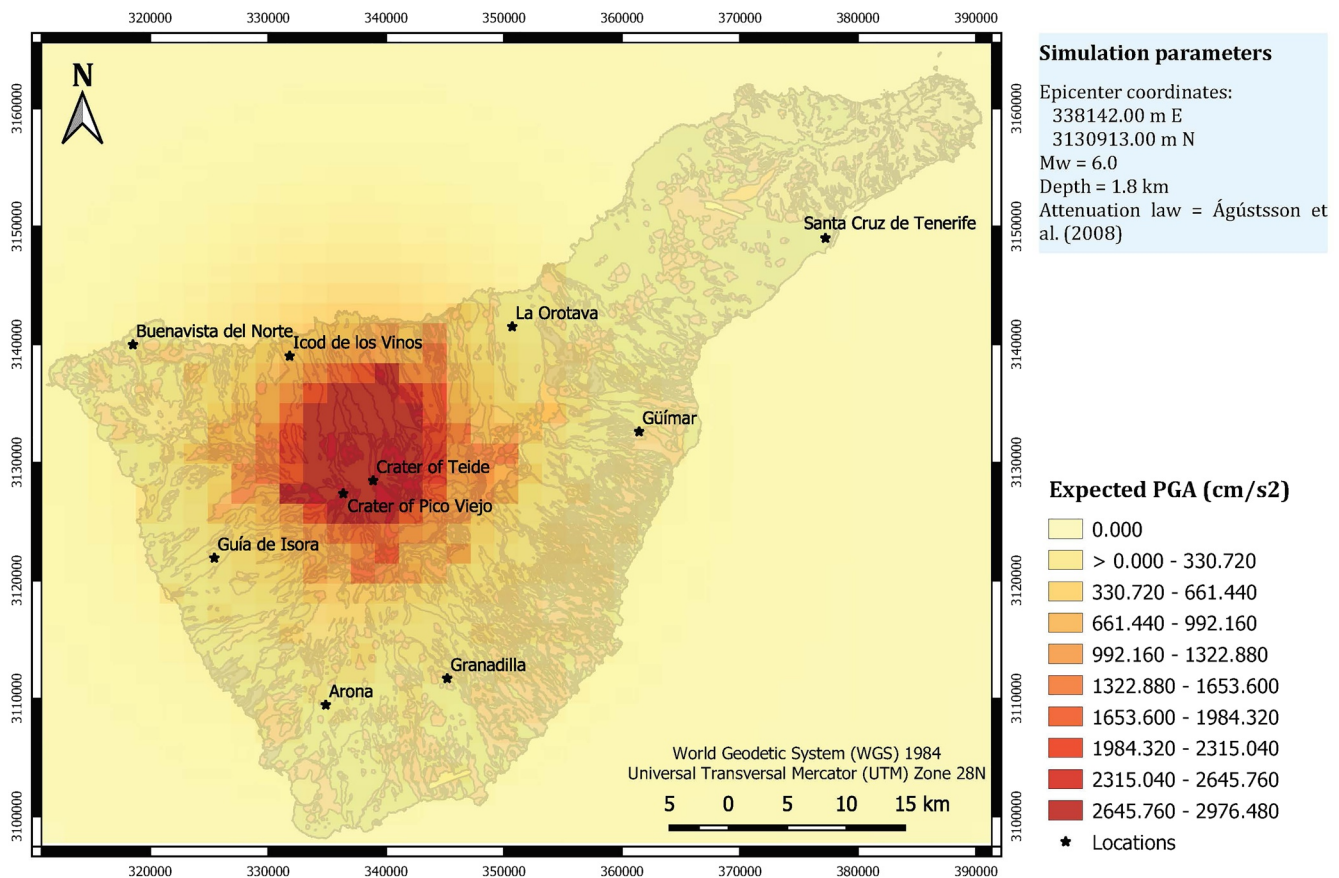


Figure 5. Expected Peak Ground Acceleration values for a M 6.0 synthetic earthquake located north of the summit of Mt Teide, Tenerife (Canary Islands), at a depth of 1.8 km, after applying the Ágústsson et al. (2008) attenuation law.

attenuation law. Thus, the lowest PGA value is 0.61 g (in case of epicenter 1), while the highest is 13.21 g (in case of epicenter 2). Therefore, the choice of one attenuation law or another, and of one epicenter or another, can vary the expected PGA value for the same M_w by up to 12.93 units.

Between these mentioned extremes, there is also a wide range of scenarios, not only in terms of maximum expected PGA values (Tables S2 and S3), but also in terms of ground response distribution (see Figures S16–S69). Deleting the depth variable, which has no influence on the results in this case, a total of 9 different scenarios were obtained per epicenter by combining only three M_w with the selected three attenuation laws. In case we could remove the attenuation law variable, if we would be able to know which one best suits the terrain of Tenerife, results would be reduced to one possibility per M_w and per epicenter. However, despite having selected only three different M_w for this study, the proposed range was between 5 and 7, a range that already includes multiple options and associated scenarios.

Apart from these results, the scenarios reveal that the areas most affected by the different earthquakes generated in this study are, in this order, the Las Cañadas caldera and its walls, the Icod valley, the NW and NE rift zones, and the area corresponding to Bandas del Sur, in the southeast of the island.

4.3. Landslide Scenarios

A total of 207 simulations was performed, six using a static analysis and 201 with a pseudo-static analysis, by applying the input parameters introduced previously to the three considered geotechnical models. The results of the slope stability analysis are shown in Figures S70–S276, and an example is given here in Figure 6; the FS values are summarized in Tables S3–S8.

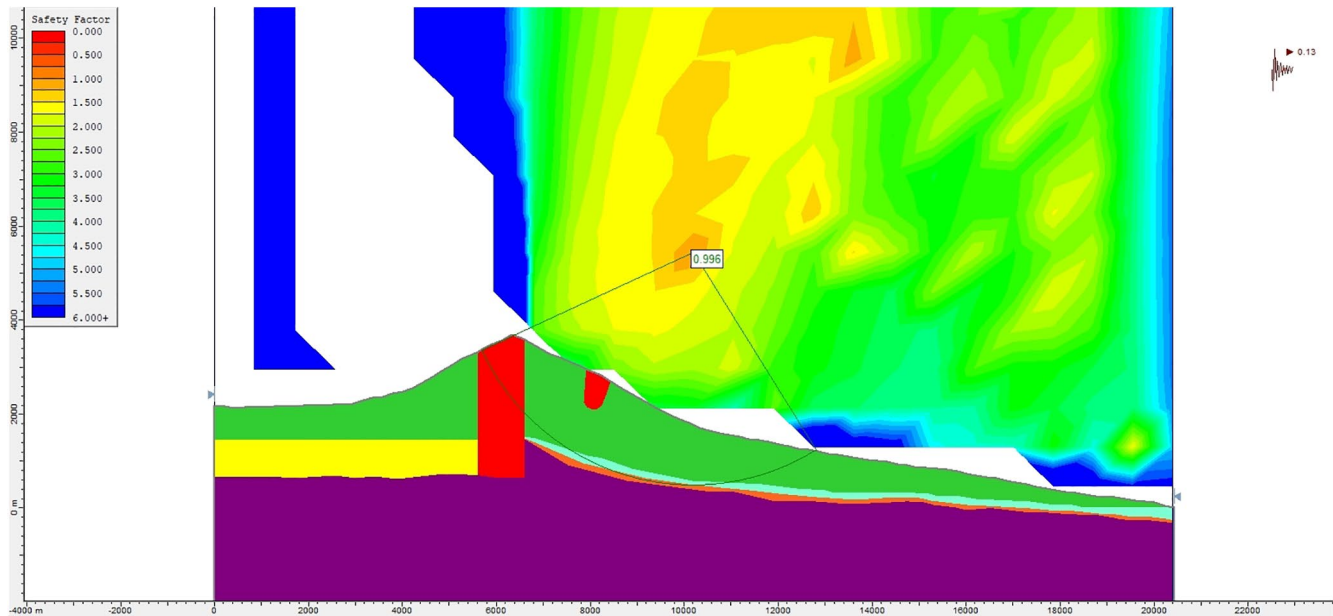


Figure 6. Slope stability pseudo-static analysis for Model 1 (with alteration zones, Figure 3a) using the Morgenstern-Price method and a k_h of 0.13. x axis corresponds to the distance in meters, with the 0 located at southern limit of the cross section represented in line I-I' shown in Figure 1, and y axis shows the altitude. The colors shown in the cross section correspond to the geotechnical units used for Model 1 and coincide with those represented in Figure 3. Colors appearing above the cross section correspond to the Factor of Safety (FS) for each area of the diagram, shown as a mirror of it. The semi-circular shape corresponds to the most probable slip surface and its FS is shown in the box, which in this case is 0.996.

All static analyses carried out for both geotechnical models give FS above 1 but below 1.5 (see Tables S4 and S5), what means that both geotechnical configurations can be considered stable under steady state conditions, that is, no earthquake. However, FS values are lower for Model 1, which has alteration zones compared to Model 2. This also holds true during pseudo-static analyses, which means that under both steady state and seismic conditions, Model 1 is slightly more unstable than Model 2 due to the presence of altered materials, which increases the instability of the area.

Under seismic conditions, the pseudo-static analyses show that Model 1 becomes unstable ($FS < 1$) at a minimum k_h of 0.1, while a minimum k_h of 0.12 and 0.28 is required for Model 2 and Model 1 Bis, respectively. This is true in case the Janbu Generalised method is applied (also Bishop simplified in case of Model 1 Bis, see Table S8), but from the results obtained it is clear that this value, which would mark the minimum required to generate instability ($FS < 1$) in the studied slope, varies from one method to another, requiring a higher k_h and, thus, a higher M_w , in case the other methods are applied to each model. This fact means that, in this study, at least three different seismic scenarios of minimum k_h required to generate instability could exist for each model. Knowing which method and which geotechnical configuration best fits the portion of the studied island, these seismic scenarios would be reduced to one.

However, even with a single minimum k_h value, there are still multiple earthquakes that could give this value. This is because if we undo the formulas of Marcuson (1981), Noda and Uwave (1976) and Saragoni (1993), applied before, to know the PGA capable of giving that value of k_h and, in turn, compare which M_w could generate that PGA, we find multiple possible seismic scenarios (see Table 4, where the minimum values of k_h discussed above have been taken as an example). This is also influenced by the location of the epicenter, as we can see in Table 4 for a PGA of 0.61 g in case of Model 1 Bis.

The generated scenarios also show the most probable failure surfaces as semicircular lines affecting the slope, with the associated FS in a box (see Figure 6). These slip surfaces show a rotational movement of the sliding block, the head of which is located south of the crater of Mt Teide in Model 1 (Figure 6) and 2. For Model 1 Bis, the head of the sliding block is located north of the Las Calvas del Teide alteration zone. For higher values of k_h these semicircular sliding surfaces become more open and wider and the head of the landslide moves northwards (see Figure S70–S276).

Table 4

Equivalences Between the Minimum Instability Values of Horizontal Acceleration (k_h) for Each Geotechnical Model and the Corresponding Peak Ground Acceleration and M_w Values

Model 1		
k_h	PGA	M_w
0.1	0.1 g (Noda & Uwave, 1976)	5.0 (Pétursson & Vogfjörð, 2009) <5.0 (Ágústsson et al., 2008) <5.0 (Beauducel et al., 2004)
	0.3 g (Marcuson, 1981)	>7.0 (Pétursson & Vogfjörð, 2009)
	0.33 g (Saragoni, 1993)	<5.0 (Ágústsson et al., 2008) >5.0 and <6.0 (Beauducel et al., 2004)
Model 2		
k_h	PGA	M_w
0.12	0.12 g (Noda & Uwave, 1976)	>5.0 and <6.0 (Pétursson & Vogfjörð, 2009) <5.0 (Ágústsson et al., 2008) 5.0 (Beauducel et al., 2004)
	0.36 g (Marcuson, 1981)	>7.0 (Pétursson & Vogfjörð, 2009)
	0.4 g (Saragoni, 1993)	<5.0 (Ágústsson et al., 2008) >5.0 and <6.0 (Beauducel et al., 2004)
Model 1 Bis		
k_h	PGA	M_w
0.28	0.61 g (Noda & Uwave, 1976)	>7.0 (Pétursson & Vogfjörð, 2009) 5.0 (<5.0 for an epicenter located on the crater) (Ágústsson et al., 2008) >5.0 and <6.0 (Beauducel et al., 2004)
	0.85 g (Marcuson, 1981)	>7.0 (Pétursson & Vogfjörð, 2009) >5.0 and <6.0 (Ágústsson et al., 2008) >6.0 and <7.0 (Beauducel et al., 2004)
	2.08 g (Saragoni, 1993)	>7.0 (Pétursson & Vogfjörð, 2009) >5.0 and <6.0 (Ágústsson et al., 2008) >7.0 (Beauducel et al., 2004)

Note. These equivalences are made with the minimum value of horizontal acceleration (k_h) at which each geotechnical model showed instability ($FS < 1$) after the analysis with SLIDE. Also shown are the PGA and M_w values after reversing the three previously applied formulas (Marcuson, 1981; Noda & Uwave, 1976; Saragoni, 1993) to each k_h and checking the possible ranges of the M_w causing these values.

All the slip surfaces generally reach the depth of the limit between the water circulation zone unit and the “Mortalón”, the latter being unaffected or only slightly affected by the potential landslide. The average maximum thickness of the potential sliding block for all models is around 500 m, but it is reduced to 300 m in case of Model 1 Bis for high k_h values.

4.4. Tsunami Scenarios

Two simulations were obtained by combining two different values for the constant retarding stress or yield strength. Tsunami simulations are shown in Movies S1 and S2, which correspond to a simulation made with a yield strength of the sliding block of 50,000 Pa and 100,000 Pa, respectively. Four different stages of the tsunami propagation are shown in Figure 7.

Both simulations give a first tsunami wave of about 200 m in height traveling northwards (Figure 7a). However, the amplitudes obtained along the affected coasts outside the impact zone are higher and slightly faster for the 100,000 Pa than for 50,000 Pa simulation. Therefore, the choice of one yield strength for the sliding block or another would vary the arrival time of the waves by about 10 s and the maximum amplitude recorded on the affected coasts by up to 50 m. In both cases, the northern and western coasts of Tenerife, the eastern coasts of La Palma and the northern coasts of La Gomera are the most affected areas of the archipelago.

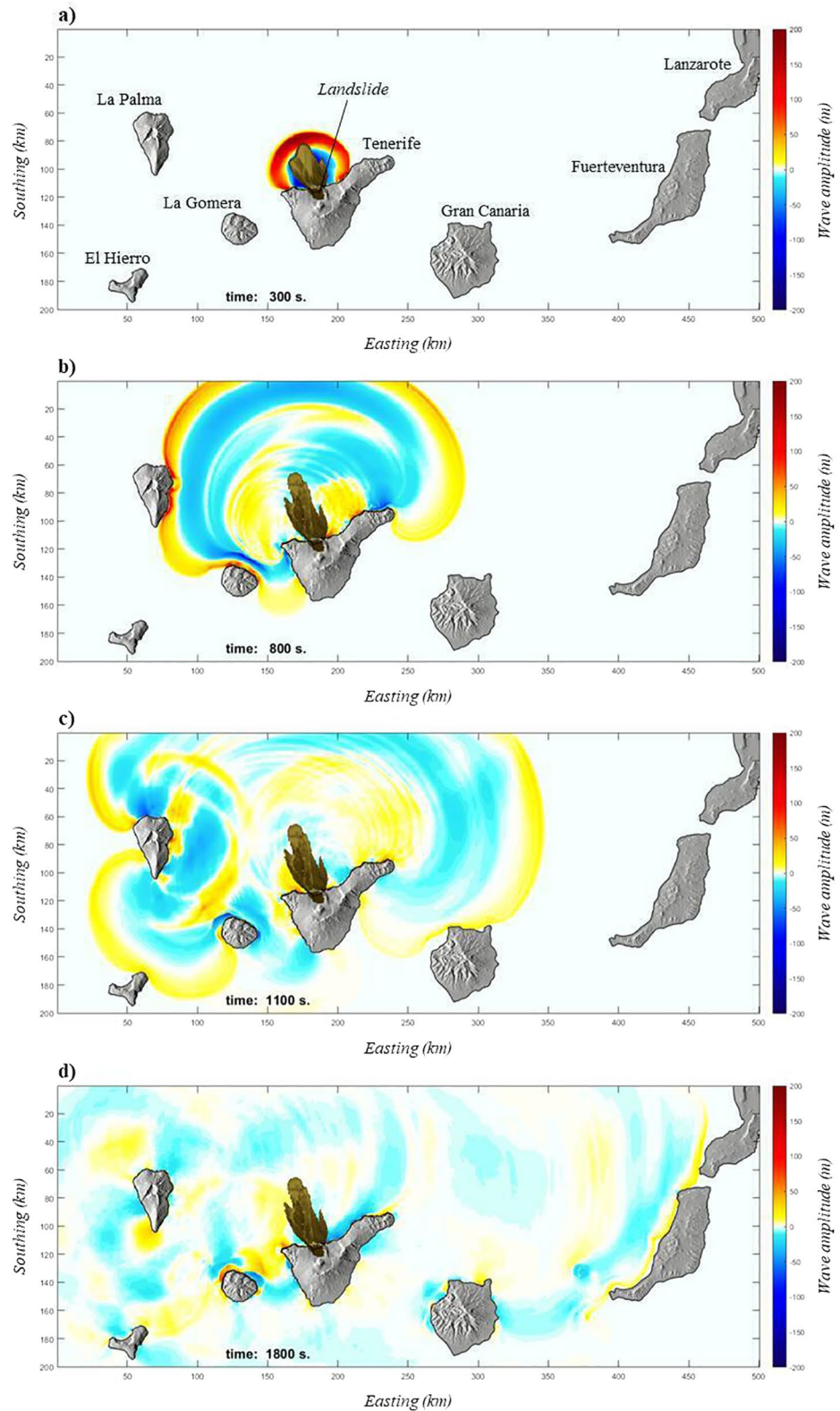


Figure 7. Simulation of the propagation of the tsunami caused by the impact of a landslide originating in the Icod valley on the ocean, with a yield strength of the sliding block of 50,000 Pa.

Considering the simulation made with 50,000 Pa, we observe that the northern coast of Tenerife is wholly affected within 580 s with a maximum amplitude of around 100 m; the exception is the municipality of Los Silos, where waves reach almost 200 m in height. This coast is hit up to nine times by waves originating from the impact of the sliding block on the ocean and by reflected waves originating after the initial impact on the eastern coast of La Palma. The western and the eastern coasts of Tenerife are completely affected after 840 s and 1,300 s. The western coast registers a maximum amplitude of 50 m, which decreases towards the south, while the eastern coast registers around 20 m. Waves coming from both sides of the island are inhibited after meeting along the southern coasts. The southern municipality of Granadilla, on the opposite coast to the landslide site, is affected after 1,070 s by the tsunami originating from the western side of the island, with a maximum amplitude of 10–15 m.

After 700 s, the north of La Gomera is the first site of the other islands of the archipelago to be hit by up to seven waves from around 80–100 m. These waves come both from the impact zone and from other islands after their reflection, especially from La Palma. The last affected island is Lanzarote, which is first hit by waves of about 25 m along its south-west coast after 1,790 s.

After 3,600 s, the ocean is still agitated around the Canary Islands and there are still maximum wave amplitudes of up to 40 m in some places. The least affected areas are the south of Gran Canaria and the eastern coasts of Fuerteventura and Lanzarote.

5. Discussion

Our objective was to identify a past extreme event in Tenerife, whose cascading sequence of hazards is known from the geology and stratigraphy of the island, and to quantify it. What we have done is to look for the most probable scenarios in case this event would be repeated today. However, multi-hazard assessments considering cascading effects are difficult to perform due to the complex relationships that can be established between different hazards, and this is a problem we had to face during this study. The lack of information and data regarding the magnitude and characteristics of each of the studied hazards (e.g., the collapse height of the PDCs, the magnitude of the seismic shocks, etc.) means that we had to work with wide ranges of input parameters. For that reason, the 277 scenarios obtained in this study were statistically analyzed to identify those combinations of parameters for each event, and those combinations of hazard scenarios, whose results best fit what happened during the El Abrigo eruption. Out of this context, all the obtained scenarios could be possible, but only few combinations of them adjust to what we observe in the geological record of the island corresponding to the El Abrigo eruption. These scenarios are discussed here.

Given that the ignimbrite resulting from the El Abrigo eruption covered nearly the whole island, the closest PDC scenario would be a collapse of the eruptive column from a height of between 2,000 and 3,000 m, with a collapse equivalent angle around 7° . In this case, nearly all the island would be hit by PDCs, and only its northeast corner would be unaffected. At the same time, or just after the emplacement of the PDCs, the caldera collapse process would begin. The resulting high magnitude seismicity would severely affect the central part of the island, corresponding to the caldera of Las Cañadas and its walls, the Icod Valley, the NE and NW rifts, and Bandas del Sur in the southeast. From a conservative point of view, and considering both the results from Hürlimann et al. (2000) and our stability analysis, if at the beginning of the collapse seismic shocks produce a PGA of around 0.3–0.33 g, an unstable state of the Icod Valley slope could be reached. Over that range of PGA, a landslide is very probable to be produced in the Icod Valley area. However, if these values of PGA are not reached at the very beginning of the collapse, but they are achieved when the process is more advanced, instability is less likely to occur as a higher PGA is required. In this case, being conservative, a landslide could be produced if a PGA between 0.61 and 0.85 g is reached during the final stages of the caldera collapse process.

The head of the landslide would be located at some point in the northern slope of Mt Teide, depending on the position of the magma chamber, as it controls the extent of the caldera collapse, and would affect an area similar to the last Icod landslide, involving a maximum thickness of 500 m. According to what is observed from the original Icod landslide deposits (Ably & Hürlimann, 2000; Watts & Masson, 2001), the sliding material would behave as a cohesive avalanche with mega-blocks, whose translational movement towards the sea would produce a 200 m-high tsunami wave in the impact area. The northern coast of Tenerife would

be devastated in less than 10 min by waves with heights of around 100–150 m (even 200 m in some places), and the rest of the islands of the Archipelago would be hit by tsunami waves up to 120 m in less than 30 min. These results are in good agreement with the geological evidence represented by the presence of tsunami deposits on the north of the island of Tenerife, at 132 m a.s.l (Paris et al., 2017). This is a reasonable approximation for the 50,000 Pa simulation, which reached 100–150 m on Tenerife. Moreover, the simulation presented also suggests that the propagation of the tsunami waves could progress beyond the limits of the Canary Islands, being potential for the impacts of such an event to be felt far from the source. However, geologic evidence has not yet identified any such distal impacts from past events, so any attempt to identify the distal limits of such tsunami remains speculative by now.

At present, the Tenerife volcanic system is not in a situation similar to that of the last caldera eruption. In fact, reaching the conditions for a caldera-forming eruption may take thousands to hundreds of thousands of years, as it requires generating a sufficient amount of eruptible phonolitic magma, and all the phonolitic eruptions occurred on Tenerife during the Holocene are too small in terms of erupted volume (Martí et al., 2008). At the current stage, the Teide and Pico Viejo complex seems still too young to reach these conditions. However, it is following a very similar evolution than the previous phonolitic cycles, and the succession of events described here is a process that has repeated several times in the past, so it is not inconsistent to consider it might occur again in the future. The occurrence of such a succession of catastrophic events do not define an scenario that can be easily managed, but identifies a possible scenario in which efforts must be invested in forecasting and prevention well in advance. In this sense, increasing the monitoring network and applying high resolution geophysical imaging methods (e.g., magnetotellurics, gravimetry, seismic tomography, etc.) of the interior of the island, able to identify and quantify the presence of fresh magma, would be potential actions to be undertaken.

In this study we have identified and quantified the main processes and characteristics of this type of extreme hazards, which reduces the uncertainty when making decisions in case we encounter a similar event in the future. For this reason, we believe that this multi-hazard assessment could help to suggest guidelines for management, monitoring and urban planning, and should be taken into account by emergency management plans designed for the Canary Islands. Despite the difficulties and the simplicity of the simulation models used, our analysis does provide significant clues that should serve to increase awareness of the potential occurrence and consequences of such large-scale events. Although our analysis could be thought of as a purely academic exercise that merely aims to increase our fund of knowledge, we believe that it will in fact help improving the current emergency management plan (PEVOLCA) by detailing appropriate hazard scenarios and optimizing mitigating actions well before any emergency caused by such extreme multi-hazard events ever occurs.

6. Conclusions

We performed a long-term volcanic multi-hazard assessment of Tenerife to predict the potential extent and impact of extreme events occurring in cascade during a caldera-forming eruption. The resulting scenarios show how large areas could be covered by PDCs (and probably associated ash fall) that would affect the main urban centers and possible evacuation routes. Furthermore, seismicity focused on the central part of the island during a caldera collapse event—that in itself could have catastrophic effects on several parts of the island—could trigger a devastating landslide in the Icod valley and produce a tsunami that would probably have a severe impact not only to the northern and western coasts of Tenerife but also to other coasts of the archipelago. This is probably the most hazardous scenario that can be envisaged for Tenerife. Fortunately, despite being possible, such scenarios only need to be anticipated with recurrences on a geological timescale; however, they should not be ignored. Over the past 1 Ma, Tenerife has experienced a cascading succession of disastrous events several times and the persistence today of the same geophysical conditions that caused them in the past means that their occurrence in the future cannot be ruled out. Therefore, improving current knowledge of the causes and mechanisms of such processes should form part of the emergency plans that are being developed to confront volcanic phenomena in the Canary Islands and other regions with similar potential problems.

Data Availability Statement

Datasets for this research are included in these papers (and their supplementary information files): Andújar et al. (2008), Carracedo et al. (2007), Coppo et al. (2008), Del Potro and Hürlimann (2008), Felpeto et al. (2007), Hernández-Gutiérrez and Santamarta (2015), Hürlimann et al. (2000), Kelfoun and Druitt (2005), Kelfoun et al. (2010), Martí (2019), Martí, Mitjavila, and Araña (1994), Núñez (2017), Pittari (2004), Pittari et al. (2008), Sheridan and Malin (1983).

Acknowledgments

This research was partially funded by the EG grant EVE (DG ECHO H2020 Ref: 826292). Marta López-Saavedra received a CSIC JAE Intro grant (JAEINT 19 01465), and an FPU PhD grant (FPU19/02413). We warmly thank the Editor Isabelle Manighetti, the Associated Editor Michael Poland, and the reviewers (Ricardo Ramalho, and an anonymous referee) for their constructive reviews and comments. We would like to thank Marc Español (CSIC) for his assistance with the computing. The text was reviewed and revised by Michael Lockwood, from Walking Catalonia.

References

- Abdel-Monem, A., Watkins, N. D., & Gast, P. W. (1972). Potassium-Argon ages, volcanic stratigraphy and geomagnetic polarity history of the Canary Islands: Tenerife, La Palma and Hierro. *American Journal of Science*, 272(9), 805–825. <https://doi.org/10.2475/ajs.272.9.805>
- Abe, K. (1992). Seismicity of the caldera-making eruption of Mount Katmai, Alaska in 1912. *Bulletin of the Seismological Society of America*, 82(1), 175–191.
- Ablay, G. J., & Hürlimann, M. (2000). Evolution of the north flank of Tenerife by recurrent giant landslides. *Journal of Volcanology and Geothermal Research*, 103(1–4), 135–159. [https://doi.org/10.1016/S0377-0273\(00\)00220-1](https://doi.org/10.1016/S0377-0273(00)00220-1)
- Ablay, G. J., & Martí, J. (2000). Stratigraphy, structure, and volcanic evolution of the Pico Teide–Pico Viejo formation, Tenerife, Canary Islands. *Journal of Volcanology and Geothermal Research*, 103(1–4), 175–208. [https://doi.org/10.1016/S0377-0273\(00\)00224-9](https://doi.org/10.1016/S0377-0273(00)00224-9)
- Ágústsson, K., Thorbjarnadóttir, B., & Vogfjörð, K. (2008). Seismic wave attenuation for earthquakes in SW Iceland: First results (Rep. 08005). Reykjavík: Icelandic meteorological office. Retrieved from <https://rafhladan.is/handle/10802/4320>
- Alvizuri, C. R., Matoza, R. S., & Okubo, P. G. (2020). Negative isotropic seismic moment tensors, migrating and cyclic seismicity during the 2018 summit collapse at Kilauea caldera. arXiv: GeophysicsarXiv:submit/3462970 [physicsgeo-ph].
- Ancochea, E., Fúster, J. M., Ibarrola, E., Cendrero, A., Coello, J., Hernan, F., et al. (1990). Volcanic evolution of the island of Tenerife (Canary Islands) in light of new K-Ar data. *Journal of Volcanology and Geothermal Research*, 44(3–4), 231–249. [https://doi.org/10.1016/0377-0273\(90\)90019-C](https://doi.org/10.1016/0377-0273(90)90019-C)
- Ancochea, E., Huertas, M. J., Cantagrel, J. M., Coello, J., Fúster, J. M., Arnaud, N., & Ibarrola, E. (1999). Evolution of the Cañadas edifice and its implications for the origin of the Cañadas Caldera (Tenerife, Canary Islands). *Journal of Volcanology and Geothermal Research*, 88(3), 177–199. [https://doi.org/10.1016/S0377-0273\(98\)00106-1](https://doi.org/10.1016/S0377-0273(98)00106-1)
- Andújar, J., Costa, F., Martí, J., Wolff, J. A., & Caroll, M. R. (2008). Experimental constraints on pre-eruptive conditions of phonolitic magma from the caldera-forming El Abrigo eruption, Tenerife (Canary Islands). *Chemical Geology*, 257(3–4), 173–191. <https://doi.org/10.1016/j.chemgeo.2008.08.012>
- Anguita, F., & Hernan, F. (1975). A propagating fracture model versus a hot spot origin for the Canary islands. *Earth and Planetary Science Letters*, 27(1), 11–19. [https://doi.org/10.1016/0012-821X\(75\)90155-7](https://doi.org/10.1016/0012-821X(75)90155-7)
- Anguita, F., & Hernan, F. (2000). The Canary Islands: A unifying model. *Journal of Volcanology and Geothermal Research*, 103(1–4), 1–26. [https://doi.org/10.1016/S0377-0273\(00\)00195-5](https://doi.org/10.1016/S0377-0273(00)00195-5)
- Araña, V. (1971). Litología y estructura del Edificio Cañadas, Tenerife (Islas Canarias). *Estudios Geológicos*, 27, 95–135.
- Araña, V., & Ortiz, R. (1991). The Canary Islands: Tectonics, magmatism and geodynamic framework. In A. B. Kampunzu, & R. T. Lubala (Eds.), *Magmatism in extensional structural settings. The Phanerozoic African plate* (pp. 209–249): Springer-Verlag. https://doi.org/10.1007/978-3-642-73966-8_9
- Asociación Española de Normalización y Certificación (AENOR). (2016). *Eurocódigo 7: Proyecto geotécnico (UNE-EN 1997-1)*: AENOR.
- Beauducel, F., Bazin, S., & Bengoubou-Valerius, M. (2004). *Loi d'atténuation B-cube pour l'évaluation rapide des intensités sismiques probables dans l'archipel de Guadeloupe (Internal Report)*. France: Institut de Physique du Globe de Paris. Retrieved from http://www.ipgp.jussieu.fr/~beaudu/download/2004_Beauducel_B3.pdf
- Bellido-Mulas, F., Gómez-Sainz de Aja, J. A., & Barrera, J. L. (2014). Mapa geológico digital continuo de España. In *GEODE (zone 2912, Canarias - Tenerife, 1:25000)*: Instituto Geológico y Minero de España (IGME). Shapefile format.
- Bishop, A. W. (1955). The use of the slip circle in the stability analysis of slopes. *Géotechnique*, 5(1), 7–17. <https://doi.org/10.1680/geot.1955.5.1.7>
- Borcherdt, R. D. (1994). Estimates of site-dependent response spectra for design (methodology and justification). *Earthquake Spectra*, 10(4), 617–653. <https://doi.org/10.1193/1.1585791>
- Boulestix, T., Hildenbrand, A., Gillot, P. Y., & Vicente-Soler, V. (2012). Eruptive response of oceanic islands to giant landslides: New insights from the geomorphologic evolution of the Teide–Pico Viejo volcanic complex (Tenerife, Canary). *Geomorphology*, 138(1), 61–73. <https://doi.org/10.1016/j.geomorph.2011.08.025>
- Bravo, T. (1962). El circo de Las Cañadas y sus dependencias. *Boletín de la Real Sociedad Española de Historia Natural*, 60, 93–108.
- Brown, R. J., Barry, T. L., Branney, M. J., Pringle, M. S., & Bryan, S. E. (2003). The Quaternary pyroclastic succession of Southeast Tenerife, Canary Islands: Explosive eruptions, related caldera subsidence, and sector collapse. *Geological Magazine*, 140(3), 265–288. <https://doi.org/10.1017/S0016756802007252>
- Bryan, S. E., Martí, J., & Cas, R. A. F. (1998). Stratigraphy of the Bandas del Sur Formation: An extracaldera record of Quaternary phonolite explosive eruptions from the Cañadas edifice, Tenerife (Canary Islands). *Geological Magazine*, 135(5), 605–636. <https://doi.org/10.1017/S0016756897001258>
- Carracedo, J. C., Day, S., Guillou, H., Rodríguez Badiola, E., Canas, J. A., & Pérez-Torrado, F. J. (1998). Hotspot volcanism close to a passive continental margin: The Canary Islands. *Geological Magazine*, 135(5), 591–604. <https://doi.org/10.1017/S0016756898001447>
- Carracedo, J. C., Guillou, H., Nomade, S., Rodríguez-Badiola, E., Pérez-Torrado, F. J., Rodríguez-González, A., et al. (2011). Evolution of ocean-island rifts: The northeast rift zone of Tenerife, Canary Islands. *Geological Society of America Bulletin*, 123(3–4), 562–584. <https://doi.org/10.1130/B30119.110.1130/b30119.1>
- Carracedo, J. C., Rodríguez-Badiola, E., Guillou, H., Paterne, M., Scaillet, S., Pérez-Torrado, F. J., et al. (2007). Eruptive and structural history of Teide Volcano and rift zones of Tenerife, Canary Islands. *Geological Society of America Bulletin*, 119(9–10), 1027–1051. <https://doi.org/10.1130/B26087.1>
- Coello, J. (1973). Las series volcánicas en subsuelos de Tenerife. *Estudios Geológicos*, 29, 491–512.

- Coppo, N., Schnegg, P. A., Heise, W., Falco, P., & Costa, R. (2008). Multiple caldera collapses inferred from the shallow electrical resistivity signature of the Las Cañadas caldera, Tenerife, Canary Islands. *Journal of Volcanology and Geothermal Research*, 170(3–4), 153–166. <https://doi.org/10.1016/j.jvolgeores.2007.09.013>
- Del Potro, R., & Hürlimann, M. (2008). Geotechnical classification and characterisation of materials for stability analyses of large volcanic slopes. *Engineering Geology*, 98(1–2), 1–17. <https://doi.org/10.1016/j.enggeo.2007.11.007>
- Edgar, C. J., Wolff, J. A., Olin, P. H., Nichols, H. J., Pittari, A., Cas, R. A. F., et al. (2007). The late Quaternary Diego Hernandez Formation, Tenerife: Volcanology of a complex cycle of voluminous explosive phonolitic eruptions. *Journal of Volcanology and Geothermal Research*, 160(1–2), 59–85. <https://doi.org/10.1016/j.jvolgeores.2006.06.001>
- Felpeo, A., Martí, J., & Ortiz, R. (2007). Automatic GIS-based system for volcanic hazard assessment. *Journal of Volcanology and Geothermal Research*, 166(2), 106–116. <https://doi.org/10.1016/j.jvolgeores.2007.07.008>
- Filson, J., Simkin, T., & Leu, L. K. (1973). Seismicity of a caldera collapse: Galapagos Islands 1968. *Journal of Geophysical Research*, 78(35), 8591–8622. <https://doi.org/10.1029/JB078i035p08591>
- Folch, A., & Martí, J. (2009). Time-dependent chamber and vent conditions during explosive caldera-forming eruptions. *Earth and Planetary Science Letters*, 280(1–4), 246–253. <https://doi.org/10.1016/j.epsl.2009.01.035>
- Fullea, J., Camacho, A. G., Negredo, A. M., & Fernández, J. (2015). The Canary Islands hot spot: New insights from 3D coupled geophysical–petrological modelling of the lithosphere and uppermost mantle. *Earth and Planetary Science Letters*, 409, 71–88. <https://doi.org/10.1016/j.epsl.2014.10.038>
- Fuster, J. M., Araña, V., Brandle, J. L., Navarro, M., Alonso, U., & Aparicio, A. (1968). *Geología y Volcanología de las Islas Canarias: Tenerife*. Instituto Lucas Mallada, CSIC.
- González de Vallejo, L., Ferrer, M., Ortuno, L., & Oteo, C. (2002). *Ingeniería Geológica*: Prentice Hall.
- Gutiérrez, F. A. (2017). *Evaluación de herramientas para el análisis de estabilidad física de una presa de relaves espesados, (Pregrade dissertation)*: University of Chile. Retrieved from Repositorio Académico de la Universidad de Chile <http://repositorio.uchile.cl/handle/2250/148601>
- Hernández-Gutiérrez, L. E., & Santamarta, J. (2015). *Ingeniería Geológica en Terrenos Volcánicos. Métodos, Técnicas y Experiencias en las Islas Canarias*. Ilustre Colegio Oficial de Geólogos. <https://doi.org/10.13140/RG.2.1.3161.6884>
- Hernández-Pacheco, A., & Ibarrola, E. (1973). Geochemical variation trends between the different Canary Islands in relation to their geological position. *Lithos*, 6(4), 389–402. [https://doi.org/10.1016/0024-4937\(73\)90055-8](https://doi.org/10.1016/0024-4937(73)90055-8)
- Hoernle, K. A. J., & Schmincke, H. (1993). The role of partial melting in the 15-Ma geochemical evolution of Gran Canaria: A blob model for the Canary hotspot. *Journal of Petrology*, 34(3), 599–626. <https://doi.org/10.1093/petrology/34.3.599>
- Huertas, M. J., Arnaud, N. O., Ancochea, E., Cantagrel, J. M., & Fuster, J. M. (2002). 40Ar/39Ar stratigraphy of pyroclastic units from the Cañadas volcanic edifice (Tenerife, Canary Islands) and their bearing on the structural evolution. *Journal of Volcanology and Geothermal Research*, 115(3–4), 351–365. [https://doi.org/10.1016/S0377-0273\(01\)00331-6](https://doi.org/10.1016/S0377-0273(01)00331-6)
- Hunt, J. E., Cassidy, M., & Talling, P. J. (2018). Multi-stage volcanic island flank collapses with coeval explosive caldera-forming eruptions. *Scientific Reports*, 8(1), 1146. <https://doi.org/10.1038/s41598-018-19285-2>
- Hunt, J. E., Wynn, R. B., Masson, D. G., Talling, P. J., & Teagle, D. A. H. (2011). Sedimentological and geochemical evidence for multistage failure of volcanic island landslides: A case study from Icod landslide on north Tenerife, Canary Islands. *Geochemistry, Geophysics, Geosystems*, 12(12), Q12007. <https://doi.org/10.1029/2011GC003740>
- Hunt, J. E., Wynn, R. B., Talling, P. J., & Masson, D. G. (2013a). Turbidite record of frequency and source of large volume (>100 km³) Canary Island landslides in the last 1.5 Ma: Implications for landslide triggers and geohazards. *Geochemistry, Geophysics, Geosystems*, 14(7), 2100–2123. <https://doi.org/10.1002/ggge.20139>
- Hunt, J. E., Wynn, R. B., Talling, P. J., & Masson, D. G. (2013b). Multistage collapse of eight western Canary Island landslides in the last 1.5 Ma: Sedimentological and geochemical evidence from subunits in submarine flow deposits. *Geochemistry, Geophysics, Geosystems*, 14(7), 2159–2181. <https://doi.org/10.1002/ggge.20138>
- Hürlimann, M., Martí, J., & Ledesma, A. (2000). Mechanical relationship between landslides and caldera collapses. *Geophysical Research Letters*, 27(16), 2393–2396. <https://doi.org/10.1029/2000GL011564>
- Ibarrola, E., Ancochea, E., Fuster, J. M., Cantagrel, J. M., Coello, J., Snelling, N. J., & Huertas, M. J. (1993). Cronoestratigrafía del Macizo de Tgaiga: Evolución de un sector del edificio Cañadas (Tenerife, Islas Canarias). *Boletín de la Real Sociedad Española de Historia Natural (Sección Geología)*, 88(1–4), 57–72.
- Iribarren, I. (2014). *Modelos geológicos en 3D de la isla de Tenerife, (Doctoral dissertation)*: Universitat de Barcelona. Retrieved from Tesis Doctorals en Xarxa (TDX) <http://hdl.handle.net/10803/284902>
- Janbu, N. (1973). Slope Stability Computations. In R. C. Hirschfeld, & S. J. Poulos (Eds.), *Embankment dam engineering* (pp. 47–86): Casagrande Volume John Wiley and Sons Inc. [https://doi.org/10.1016/0148-9062\(75\)90139-4](https://doi.org/10.1016/0148-9062(75)90139-4)
- Kelfoun, K., & Druitt, T. H. (2005). Numerical modeling of the emplacement of Socompa rock avalanche, Chile. *Journal of Geophysical Research*, 110(B12), 1–13. <https://doi.org/10.1029/2005JB003758>
- Kelfoun, K., Giachetti, T., & Labazuy, P. (2010). Landslide-generated tsunamis at Réunion Island. *Journal of Geophysical Research*, 115(F4). <https://doi.org/10.1029/2009JF001381>
- Lee, B., Preston, F., & Green, G. (2012). *Preparing for high-impact, low-probability events: Lessons from Eyjafjallajökull*: Chatham House.
- Lo Giudice, E., & Rasa, R. (1992). Very shallow earthquakes and brittle deformation in active volcanic areas. The Etnean region as an example. *Tectonophysics*, 202(2–4), 257–268. [https://doi.org/10.1016/0040-1951\(92\)90111-I](https://doi.org/10.1016/0040-1951(92)90111-I)
- Malin, M. C., & Sheridan, M. F. (1982). Computer-assisted mapping of pyroclastic surges. *Science*, 217(4560), 637–640. <https://doi.org/10.1126/science.217.4560.637>
- Marcuson, W. F. (1981). Moderator's report for session on Earth dams and stability of slopes under dynamic loads. *Proceedings of the International Conference on Recent Advances In Geotechnical Earthquake Engineering and Soil Dynamics* (Vol. 3).
- Marrero, R. (2010). *Modelo hidrogeoquímico del acuífero de Las Cañadas del Teide, Tenerife, Islas Canarias, (Doctoral dissertation)*: Universitat Politècnica de Catalunya. Retrieved from Tesis Doctorals en Xarxa (TDX) <http://hdl.handle.net/10803/6277>
- Martí, J. (2019). Las Cañadas caldera, Tenerife, Canary Islands: A review, or the end of a long volcanological controversy. *Earth-Science Reviews*, 196, 102889. <https://doi.org/10.1016/j.earscirev.2019.102889>
- Martí, J., Ablay, J., Redshaw, L. T., & Sparks, R. S. J. (1994). Experimental studies of collapse calderas. *Journal of the Geological Society*, 151(6), 919–929. <https://doi.org/10.1144/gsjgs.151.6.0919>
- Martí, J., Geyer, A., Folch, A., & Gottsmann, J. (2008). Chapter 6 A review on collapse caldera modelling. *Developments in Volcanology*, 10, 233–283. [https://doi.org/10.1016/S1871-644X\(07\)00006-X](https://doi.org/10.1016/S1871-644X(07)00006-X)

- Martí, J., & Gudmundsson, A. (2000). The Las Cañadas caldera (Tenerife, Canary Islands): An overlapping collapse caldera generated by magma-chamber migration. *Journal of Volcanology and Geothermal Research*, 103(1–4), 161–173. [https://doi.org/10.1016/S0377-0273\(00\)00221-3](https://doi.org/10.1016/S0377-0273(00)00221-3)
- Martí, J., Hürlimann, M., Ablay, G. J., & Gudmundsson, A. (1997). Vertical and lateral collapses on Tenerife (Canary Islands) and other volcanic ocean islands. *Geology*, 25(10), 879–882. [https://doi.org/10.1130/0091-7613\(1997\)025<0879:valcot>2.3.co;2](https://doi.org/10.1130/0091-7613(1997)025<0879:valcot>2.3.co;2)
- Martí, J., Mitjavila, J., & Araña, V. (1994). Stratigraphy, structure and geochronology of the Las Cañadas caldera (Tenerife, Canary Islands). *Geological Magazine*, 131(6), 715–727. <https://doi.org/10.1017/S0016756800012838>
- McGuire, W. J., Pullen, A. D., & Saunders, S. J. (1990). Recent dyke-induced large-scale block movement at Mount Etna and potential slope failure. *Nature*, 343(6256), 357–359. <https://doi.org/10.1038/343357a0>
- Ministerio de Fomento. (2006). *Documento básico de Seguridad estructural. Código técnico de la Edificación (CTE)*: Ministerio de Fomento. Retrieved from <https://www.codigotecnico.org/>
- Mitjavila, J., & Villa, I. M. (1993). Temporal evolution of the Diego Hernandez Formation (Las Canadas, Tenerife) and confirmation of the age of the caldera using the 40Ar/39Ar method. *Revista de la Sociedad Geológica de España*, 6(1–2), 61–65.
- Morgenstern, N. R., & Price, V. E. (1965). The analysis of the stability of general slip surfaces. *Géotechnique*, 15(1), 79–93. <https://doi.org/10.1680/geot.1965.15.1.79>
- Noda, S., & Uwawe, T. (1976). *Relation between seismic coefficient and ground acceleration for gravity quaywalls*. Paper presented at the 6th World Conference on Earthquake Engineering, the Indian Society of Earthquake Technology.
- Nott, J. (2006). *Extreme events: A physical reconstruction and risk assessment*: Cambridge University Press. <https://doi.org/10.1017/CBO9780511606625>
- Núñez, A. (2017). *Simulación de escenarios sísmicos mediante un Sistema de Información Geográfica para la Península Ibérica, las Islas Baleares y las Islas Canarias, considerando el efecto de sitio y las dimensiones y características de la fuente sísmica, (Doctoral dissertation)*: Universidad Politécnica de Madrid. Retrieved from Dialnet <https://dialnet.unirioja.es/servlet/tesis?codigo=185118>
- Paris, R., Coello-Bravo, J. J., Martín-González, M. E., Kelfoun, K., & Nauret, F. (2017). Explosive eruption, flank collapse and megatsunami at Tenerife ca. 170 ka. *Nature Communications*, 8(1), 15246. <https://doi.org/10.1038/ncomms15246>
- Patrick, M. R., Houghton, B. F., Anderson, K. R., Poland, M. P., Montgomery-Brown, E., Johanson, I., et al. (2020). The cascading origin of the 2018 Kilauea eruption and implications for future forecasting. *Nature Communications*, 11, 5646. <https://doi.org/10.1038/s41467-020-19190-1>
- Pétursson, G. G., & Vogfjörð, K. S. (2009). *Attenuation relations for near- and far-field peak ground motion (PGV, PGA) and new magnitude estimates for large earthquakes in SW-Iceland* (Rep. VI 2009-012). Reykjavík: Icelandic meteorological office. Retrieved from http://www.vedur.is/media/vedurstofan/utgafa/skyrslur/2009/VI_2009_012.pdf
- Pittari, A. (2004). *Eruption dynamics and emplacement processes for the climatic Abrigo member, Tenerife, Canary Islands, (Doctoral dissertation)*: Retrieved from Hargrave-Andrew Library Monash University. <https://monash.hosted.exlibrisgroup.com/permalink/f/31uhmh/catau21136929030001751>
- Pittari, A., Cas, R. A. F., Wolff, J. A., Nichols, H. J., Larson, P. B., & Martí, J. (2008). The use of lithic clast distributions in pyroclastic deposits to understand pre- and syn-caldera collapse processes: A case study of the Abrigo Ignimbrite, Tenerife, Canary Islands. In J. Gottsmann, & J. Martí (Eds.), *Caldera volcanism: Analysis, modelling and response* (pp. 97–142): Elsevier. [https://doi.org/10.1016/S1871-644X\(07\)00003-4](https://doi.org/10.1016/S1871-644X(07)00003-4)
- Plag, H. P., Stein, S., Brocklebank, S., Jules-Plag, S., Marsh, S., & Campus, P. (2013). *Extreme geohazards: Reducing the disaster risk and increasing resilience*. European Science Foundation.
- Ranke, U. (2016). *Natural disaster risk management*: Springer. <https://doi.org/10.1007/978-3-319-20675-2>
- Riel, B., Milillo, P., Simons, M., Lundgren, P., Kanamori, H., & Samsonov, S. (2015). The collapse of Bardarbunga caldera, Iceland. *Geophysical Journal International*, 202(1), 446–453. <https://doi.org/10.1093/gji/ggv157>
- Rocscience Inc. (2020). *Slide2*. Retrieved from <https://www.rocscience.com/software/slide2>
- Saragoni, G. (1993). Análisis del riesgo sísmico para la reconstrucción del puerto de Valparaíso. In Matemáticas (Ed.), *Asociación Chilena de Sismología e Ingeniería Antisísmica, Universidad de Chile, Facultad de Ciencias Físicas y. Proceedings of the Sixth Chilean Conference on Seismology and Earthquake Engineering* (pp. 165–178): The Association.
- Schmincke, H. (1982). Volcanic and geochemical evolution of the Canary Islands. In U. von Rad, K. Hinz, M. Sarnthein, & E. Siebold (Eds.), *Geology of the Northwest African continental margin* (pp. 273–306): Springer-Verlag. https://doi.org/10.1007/978-3-642-68409-8_12
- Sharma, A. S., Baker, D. N., Bhattacharyya, A., Bunde, A., Dimri, V. P., Gupta, H. K., et al. (2012). Complexity and extreme events in Geosciences: An overview. In A. S. Sharma, A. Bunde, V. Dimri, & D. N. Baker (Eds.), *Extreme events and natural hazards: The complexity perspective. Geophysical monograph series* (Vol. 196, pp. 1–16): American Geophysical Union. <https://doi.org/10.1029/2012GM001233>
- Sheridan, M. F., & Malin, M. C. (1983). Application of computer-assisted mapping to volcanic hazard evaluation of surge eruption: Vulcano, Lipari, Vesuvius, explosive volcanism. *Journal of Volcanology and Geothermal Research*, 17(1–4), 187–202. [https://doi.org/10.1016/0377-0273\(83\)90067-7](https://doi.org/10.1016/0377-0273(83)90067-7)
- Thirlwall, M. F., Singer, B. S., & Marriner, G. F. (2000). 39Ar/40Ar ages and geochemistry of the basaltic shield stage of Tenerife, Canary Islands, Spain. *Journal of Volcanology and Geothermal Research*, 103(1–4), 247–297. [https://doi.org/10.1016/S0377-0273\(00\)00227-4](https://doi.org/10.1016/S0377-0273(00)00227-4)
- Toyos, G. P., Cole, P. D., Felpeto, A., & Martí, J. (2007). A GIS-based methodology for hazard mapping of small pyroclastic density currents. *Natural Hazards*, 41(1), 99–112. <https://doi.org/10.1007/s11069-006-9026-9>
- Uriel, S., & Serrano, A. (1975). Propiedades geotécnicas de algunos aglomerados volcánicos, en las Islas Canarias. In Simposio Nacional sobre Rocas Blandas. *Memorias del Simposio Nacional sobre Rocas Blandas* (tomo I, A-10): Sociedad Española de Mecánica de Rocas.
- Voight, B., & Elsworth, D. (1997). Failure of volcano slopes. *Géotechnique*, 47(1), 1–31. <https://doi.org/10.1680/geot.1997.47.1.1>
- Watts, A., & Masson, D. G. (2001). New sonar evidence for recent catastrophic collapses of the north flank of Tenerife, Canary Islands. *Bulletin of Volcanology*, 63(1), 8–19. <https://doi.org/10.1007/s004450000119>